Optics Communications 283 (2010) 1849–1853

Contents lists available at ScienceDirect

Optics Communications

journal homepage: www.elsevier.com/locate/optcom

An etalon-based method for frequency calibration of terahertz time-domain spectrometers (THz TDS)

M. Naftaly [a,*], R.A. Dudley [a], J.R. Fletcher [b]

[a] National Physical Laboratory, TQEM, Hampton Road, Teddington, Middlesex TW11 0LW, UK
[b] Department of Physics, Durham University, Durham, UK

ARTICLE INFO

Article history:
Received 17 July 2009
Received in revised form 27 November 2009
Accepted 11 December 2009

ABSTRACT

We present an etalon-based method of calibrating the frequency of terahertz time-domain spectrometers (THz TDS). The method utilizes the etalon effect produced by multiple reflections in non-absorbing wafers or in narrow air–gaps. The technique provides frequency calibration across the measurement band with uncertainties comparable with the typical THz TDS resolution.

Crown Copyright © 2009 Published by Elsevier B.V. All rights reserved.

1. Introduction

The terahertz time-domain spectrometer (THz TDS) has emerged as a key measurement device for spectroscopic investigations in the frequency range of 0.1–3 THz [1–3]. Measurements with a TDS are made in the time domain, typically in conjunction with electro-optic sampling for signal detection. Conversion from the time-domain data to a frequency spectrum is achieved by applying the Fourier Transform, calculated numerically using the Fast Fourier Transform (FFT) algorithm.

A THz TDS may suffer from several sources of frequency error, including: delay line positioning errors, chirp of the THz and/or probe pulse, and various sources of spatial beam distortion affecting the pump–probe overlap [4]. Applying FFT to the data tends to amplify the effect of these errors, and produces frequency uncertainties that are difficult to quantify. Although a formalism capable of quantifying such errors has been developed [5], and calibrating the frequency scale of a THz TDS is in principle possible by adopting techniques used in high-speed electrical signal calibration [6], in practice these techniques and calculations are difficult, and it remains far easier, quicker and more reliable in the context of a TDS to use a calibration standard.

Perhaps the most widely used means of frequency verification in the THz band is atmospheric water vapor which possesses many strong narrow lines. However, although the frequencies of these lines are well known [7,8], their relative amplitudes vary with environmental conditions [9] such as atmospheric pressure and humidity. This makes it difficult to compare spectra obtained on different occasions or in different labs. Moreover, many of the lines are doublets and triplets, and therefore require very high (sub-GHz) frequency resolution to define their peak maxima and profiles. The spacing of lines is particularly dense at higher frequencies above 2 THz, where the reduced signal-to-noise ratio and dynamic range of a TDS make accurate measurements far more difficult, and densely spaced peaks challenging to define.

A calibration device that produces regularly spaced peaks across the entire THz band, of a uniform size and having a well-defined profile, would therefore be advantageous. We describe the use of the etalon effect as a calibration method that offers such frequency scale.

2. Terahertz TDS

The TDS at the National Physical Laboratory follows the design of many other groups [10,11], incorporating a femtosecond laser, a 300 mm long optical delay line, a biased GaAs emitter, electro-optic detection using a ⟨1 1 0⟩ ZnTe crystal, and a configuration of four 90° parabolic mirrors to guide THz radiation. In the described experiments, data acquisition was achieved by sweeping, rather than stepping, the delay line, allowing for faster scan times.

In the simplest approach, the frequency resolution of a TDS system can be taken as the step size of the FFT data set Δf_{TDS}, given by $\Delta f_{TDS} = c/2L$, where L is the length of the delay sweep. In principle, given an arbitrarily long delay line, the resolution of a TDS is ultimately limited by the repetition rate of the pump laser, which is typically around 80 MHz for femtosecond lasers. However, in practice the achievable resolution is much lower and is set by the noise floor of the system [12]. In common experimental practice, the maximum sweep length L_{max} is the delay where the THz signal remains at least a factor of 2 above the noise floor of the detector. In the case of the NPL TDS this extends beyond 100 mm, allowing a frequency resolution of 1.5 GHz to be achieved.

The frequency scale of the TDS is obtained from the position of the optical delay line. Therefore the minimum frequency

* Corresponding author. Tel.: +44 208 943 8787.
E-mail address: mira.naftaly@npl.co.uk (M. Naftaly).

0030-4018/$ - see front matter Crown Copyright © 2009 Published by Elsevier B.V. All rights reserved.
doi:10.1016/j.optcom.2009.12.025

uncertainty is determined by the uncertainty in the displacement of the delay line. However, in practice the amplitude noise in the data distorts peak profiles and their apparent positions, and so limits the achievable frequency uncertainty.

In TDS systems, both the dynamic range and the signal-to-noise ratio decrease steeply with frequency [11], causing an increased error in the peak positions.

3. TDS frequency test using etalon

A potentially self-contained test capable of verifying the frequency scale and the spectral amplitude profile of TDS systems can be performed using a simple etalon-based technique. The test utilizes the occurrence of secondary peaks produced by multiple reflections in thin plane-parallel samples inserted in the THz beam.

It is a well-known phenomenon in TDS systems that multiple reflections in plane-parallel thin samples give rise to etalon-like oscillations in the calculated spectrum. The problem of removing these oscillations from the measured spectra has been extensively addressed and a number of solutions suggested [13–15]. Here etalon oscillations are utilized for the verification of the TDS frequency and amplitude scales.

The method is based on the fact that etalon peaks and troughs in the calculated spectrum occur at frequencies of [16]

$$\begin{aligned} f_N &= \tfrac{c}{2nl}N \quad \text{(peaks)} \\ f_{N+1/2} &= \tfrac{c}{2nl}(N+\tfrac{1}{2}) \quad \text{(troughs)} \end{aligned} \tag{1}$$

where n is the refractive index of the etalon material and l is its thickness. The integer N is the order of the peak, corresponding to the number of wavelengths in a CW etalon. If the sample thickness and refractive index are known, the order N can be identified, and the peak frequencies calculated.

Two types of etalon must be considered: air–gap and solid wafer. Both have respective advantages and drawbacks. It must be noted, however, that in both cases the frequency resolution is limited by the low finesse, which arises from the requirement that the etalon transmission must be sufficiently high to allow measurement of the main pulse and at least one pulse echo with a good signal-to-noise ratio (SNR). In practice, this limits the finesse to < 5.

An air–gap etalon consists of two partially reflecting plates separated by a fixed-thickness spacer. It has the advantage that the refractive index in Eq. (1) is that of air and thus well known. For all except very high-resolution measurements, a refractive index of 1 may be assumed. Frequency calibration using an air–gap etalon is therefore self-contained and potentially traceable. On the other hand, such an etalon must be carefully engineered and maintained in order to preserve its spacing to a high accuracy, and may also be sensitive to temperature variations and atmospheric humidity. Several issues must be considered in selecting the etalon plates. These must be highly transparent (i.e. non-absorbing and non-scattering) and thick enough to avoid plate echoes being included in the pulse train. Plates may be metal-coated, or made from a high refractive index material, such as silicon. Coated polymer plates have the advantage of reduced plate echoes; however, low-reflectance metal coating is fragile and susceptible to environmental damage. Uncoated plates of sufficient thickness may provide a more convenient and less expensive engineering solution to a stable, rigid and robust air–gap etalon.

An alternative type of etalon is a solid wafer made from a THz-transparent, high refractive index material. Examples of such materials include high-resistivity Si, GaAs and Ge. Such wafers are inexpensive to obtain and relatively insensitive to environmental factors. Their main disadvantage is that the refractive index must be independently measured or otherwise known. Although the refractive index can be calculated directly from the time-domain data (provided that the wafer thickness is accurately known), in TDS both the frequency spectrum and the refractive index are derived from the position of the delay line [1–3], so the two quantities are subject to common-mode uncertainties in the position measurement.

The two parameters contributing to the uncertainty in the calculated frequency in Eq. (1) are the wafer thickness and the refractive index. The combined uncertainty in the peak/trough frequency interval $f = c/2nl$ is therefore [17]:

$$\begin{aligned} \tfrac{\Delta f}{f} &= \tfrac{\Delta l}{l} \quad \text{air—gap} \\ \tfrac{\Delta f}{f} &= \sqrt{\left(\tfrac{\Delta n}{n}\right)^2 + \left(\tfrac{\Delta l}{l}\right)^2} \quad \text{solid wafer} \end{aligned} \tag{2}$$

The resulting error in the calculated peak position is cumulative, equal to the interval error times peak order, and will appear as a systematic linearly increasing shift in the observed peak position relative to the calculated value. Refractive indices are commonly quoted in the literature with an uncertainty of <0.0001 [18,19]. In comparison, the uncertainty in the etalon thickness is limited by the achievable wedge angle and flatness of the wafer or spacer, and is typically of the order of 2 μm. An air–gap etalon would use a spacer of ~2 mm width, while a wafer etalon would be ~0.5 mm thick. Therefore the uncertainty in the calculated etalon frequencies for both types of etalon is dominated by its thickness, so that $\Delta f/f \cong \Delta l/l$.

Provided that the frequency scale of a TDS is correct, the largest sources of error in the measured peak/trough frequencies are the resolution of the system and the frequency-dependent noise in the data, both of which are expected to be randomly distributed around zero. In contrast, an error in the frequency scale would manifest as a linearly increasing deviation from the calculated peak/trough values. This means that an error in the frequency scale cannot be distinguished from an error in the etalon thickness (see Eq. (1)). Therefore for calibration purposes the thickness of the etalon at the point where it is transected by the THz beam must be known with the highest achievable accuracy, preferably such that the frequency uncertainty (see Eq. (2)) is $\Delta f < \Delta f_{TDS}$.

Additional information is provided by the transmission profile. The amplitude transmission spectrum of a zero-loss (non-absorbing, non-scattering) etalon as a function of frequency f is given by [16]:

$$\begin{aligned} T_{\text{wafer}} &= (1 + F\sin^2\tfrac{\delta}{2})^{-1/2} \\ T_{\text{air—gap}} &= (1 + F\sin^2\tfrac{\delta}{2})^{-1/2} R \\ F &= \tfrac{4R}{(1-R)^2} \\ R &= \left(\tfrac{n-1}{n+1}\right)^2 \\ \delta_{\text{wafer}} &= 4\pi nlf/c \\ \delta_{\text{air—gap}} &= 4\pi lf/c \end{aligned} \tag{3}$$

The peak/trough frequencies can provide frequency calibration, while the transmission spectrum can verify the measurement of the spectral amplitude profile. It is also possible to derive the refractive index from the spectral profile of the etalon transmission function by fitting Eq. (3) to the data based only on the sample thickness. It must be noted, however, that this procedure is warranted only if the linearity of the amplitude measurement has been independently tested and confirmed [7]. Nevertheless, such fitting of frequency to the model of Eq. (3) using only sample thickness can in principle provide a route for a self-contained traceable frequency calibration of a TDS [20]. The main difficulty in this procedure is that the accuracy of the refractive index fit may be relatively low, unless the data have a very high SNR.

4. Results

In order to produce correct frequency calibration, the etalon must be positioned at zero angle of incidence to the THz beam. Non-zero incidence causes errors due to the increase in the optical path through the etalon and its effect on the spacing of the peaks/troughs. The angle sensitivity is therefore weak, and satisfactory alignment is easily achieved. For example, at the frequency of 1 THz, the error is 0.01 GHz at 1° incidence and 1 GHz at 10°.

In carrying out frequency calibration measurements, it is important to avoid distorting the THz beam, since studies have shown that measured spectra may be significantly distorted by strong focusing [21]. The errors arising from beam distortion are difficult to quantify, but are expected to be small in most cases, and negligible if the THz beam is approximately collimated. Accordingly, all described data were obtained by placing the etalons in the collimated part of the THz beam path.

Three etalons were used in the experiments, two Si wafers and an air–gap. The air–gap consisted of a 2165 ± 7 μm thick spacer and two uncoated optically polished Si plates each 3 mm thick. One of the wafers was 50 mm in diameter, optically polished on both sides, with thickness that varied across its area from 500 ± 2 μm to 520 ± 2 μm. The thickness of the central area transected by the THz beam was 509 ± 2 μm. The second wafer was 75 mm in diameter, 438 ± 2 μm thick, and was polished on one side and ground on the other. Since the refractive index of Si is 3.4175 [19], all three etalons therefore had a finesse of 2.5 (assuming zero-loss surfaces). The free spectral ranges expected in the three etalons were: 69.3 ± 0.2 GHz in the air–gap; 86 ± 1 GHz in the 50 mm wafer; and 100.2 ± 0.5 GHz in the 75 mm wafer.

The TDS frequency resolution, taken as the FFT step size, was 2 GHz in measurements on wafers, and 15 GHz in measurements on the air–gap etalon. The air–gap data had a lower resolution because it was necessary to restrict the scan length so as to exclude echoes arising within the plates. Fig. 1 presents the time-domain data for the air–gap etalon, showing the main THz peak, two etalon echoes, and an echo arising from reflections within the plates. Also indicated is the measurement window, which limits the available sweep length and therefore the frequency resolution. The resolution may be improved by using thicker end-plates which would allow a longer sweep length.

Fig. 2a and b shows a section of the etalon transmission spectrum for the polished Si wafer and the air–gap etalon respectively. Also included is the model calculated from Eq. (3) using the refractive index and the etalon thickness as input parameters. The model uses the frequency scale of the relevant data set, for easier point-by-point comparison with the experimental data. It is seen that in both cases the agreement between the data and the model is very good. It is important to note that the model in Fig. 2 is not fitted to the data, but is calculated directly using the known etalon properties. Therefore the close agreement between the data and the model serves to confirm the correctness of both the frequency scale and the amplitude measurement of the TDS.

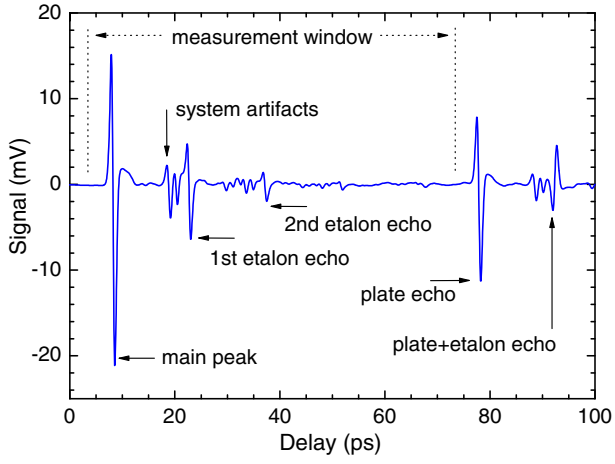

Fig. 1. The time-domain trace for the air–gap etalon (System artifacts are caused by echoes in the optical elements of the TDS system).

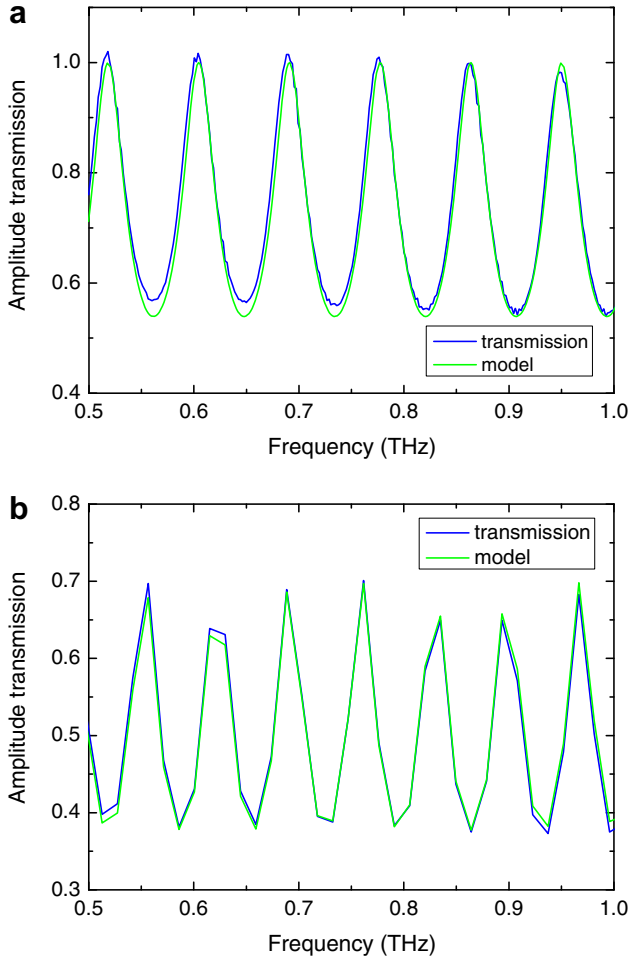

Fig. 2. Part of the etalon transmission spectrum together with the model. (a) Si wafer; (b) air–gap. The model is calculated from Eq. (3) using the etalon thickness and refractive index as input parameters, and the frequency scale of the relevant data set (the model is not fitted to the data).

The simplest and most straightforward method of analyzing the spectral data for the purpose of frequency calibration is as follows. Note the frequencies of the peaks and troughs in the transmission spectrum of the etalon obtained via the usual FFT. Then calculate the expected peak/trough frequencies of the etalon from Eq. (1) based on the known etalon thickness, and in the case of a wafer, its refractive index. A comparison of the two data sets will yield the difference between the measured and expected frequency value for each peak/trough. It is helpful to display the results by plotting these differences, i.e. the frequency errors, as a function of the etalon peak/trough position, as shown in Fig. 3. Such a plot would reveal any systematic frequency error, as well as the digitizing errors and the noise in the data. It also helps to identify the band over which frequency measurements are valid within a defined uncertainty.

As seen in Fig. 3, in all etalon measurements the frequency errors are distributed evenly around zero, confirming that there is

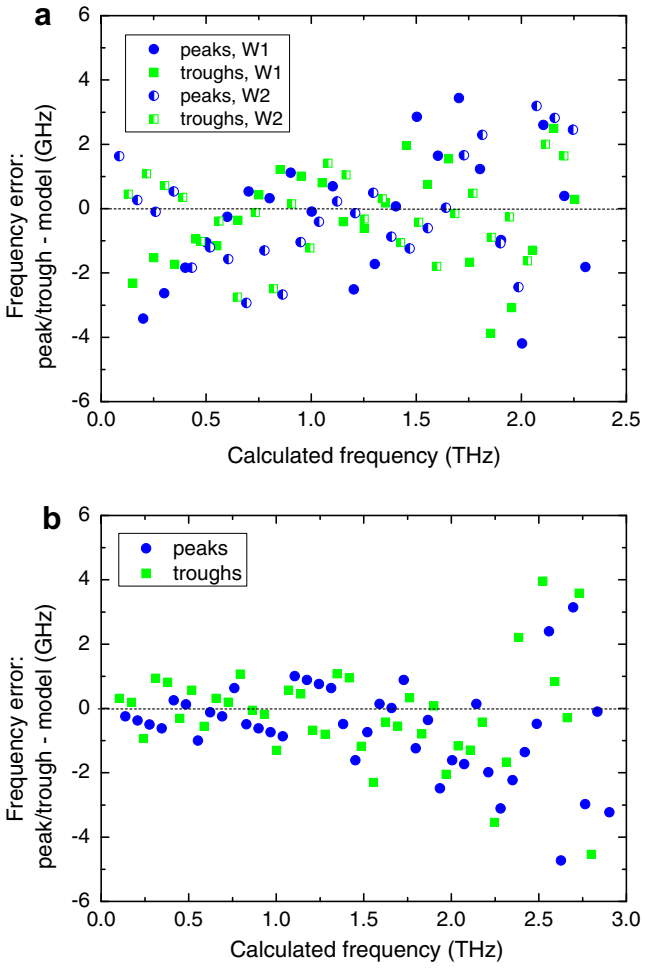

Fig. 3. Differences between the measured and calculated peak/trough frequencies. (a) Si wafers: W1 polished on both sides, W2 polished on one side; (b) air–gap etalon.

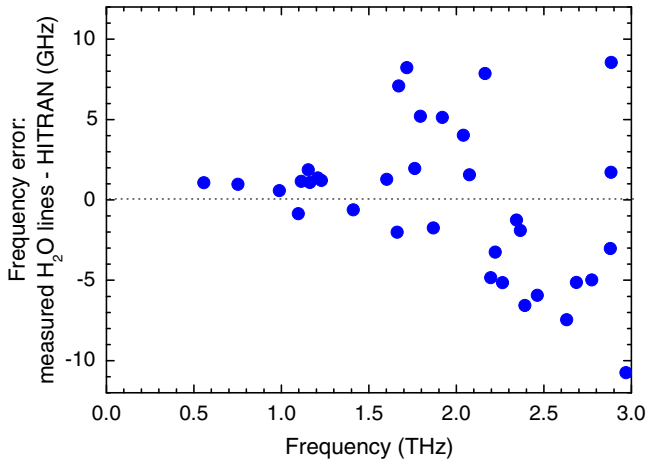

Fig. 4. Differences between the peak frequencies of H_2O lines as measured and those given by the HITRAN database.

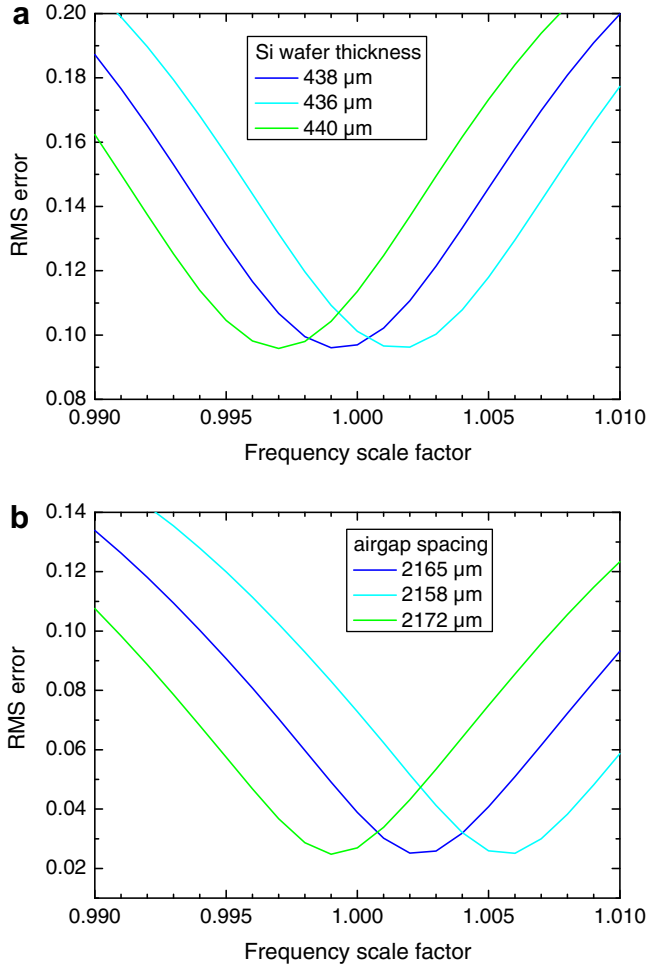

Fig. 5. RMS error as a function of the scaling factor. Separate lines show the model calculated assuming the etalon thickness plus/minus the thickness uncertainty. (a) Si wafer (semi-polished), 438 ± 2 μm thick; (b) air–gap, 2165 ± 7 μm thick.

no systematic frequency error in the system and that the errors arise from noise. The magnitude of the errors at frequencies below 2 THz is comparable with the FFT step size (2 GHz) in the case of Si wafers. In the case of the air–gap etalon, the errors are significantly smaller than the step size (15 GHz), reflecting the fact that peak/trough positions can be defined to a better accuracy than the step size of the data set; however, the digitizing error is clearly seen. Notably, Fig. 3a shows no significant difference between the polished and semi-polished wafers, and therefore demonstrates that even an imperfect etalon whose reflectivity is reduced by scattering losses nevertheless provides a good calibration device. In both figures the errors are seen to increase at higher frequencies, as the dynamic range of the TDS decreases and the system approaches its noise floor. The average magnitude of errors demonstrates the accuracy of frequency measurement over different frequency bands.

Calibration using etalon may be compared with that using water vapour, which is the most widely employed technique. To this purpose, Fig. 4 plots the differences between the measured water lines and those given by the HITRAN database [22]. The measurement of the water lines was carried out with the same resolution as the etalon measurements. It is seen that water lines provide no calibration below 0.5 THz and offer only a few lines between 0.5 and 1.5 THz. Moreover, the errors at frequencies above 1.5 THz are several times larger than those obtained using either solid or air–gap etalon, as seen in Fig. 3.

A more accurate, although more elaborate and computation-intensive, analysis of the data can be obtained by applying a form of least-squares (χ^2) fitting [17], i.e. by calculating the root-mean-square (RMS) difference between the model and measured transmission, and then minimizing it by applying a frequency-scaling

factor. As previously, the input parameters of the model are the etalon thickness and the refractive index of the etalon material; and the expected etalon transmission spectrum is calculated from Eq. (3). The RMS error is computed by taking the squared difference between calculated and measured transmission at each data point, and summing these over a selected frequency range. The measured spectrum is then scaled by multiplying its frequency axis by a factor that is close to but not equal to unity; and the RMS error is recalculated for this value of the scaling factor. Minimizing the RMS error by varying the scaling factor identifies the true frequency calibration of the TDS being tested. A correct TDS frequency scale will produce a minimum at 1, as demonstrated in Fig. 5. The width of the minimum gives an indication of the accuracy of the calibration factor. The method is relatively insensitive to variations in amplitudes of the maxima and minima of transmission, although these will be reflected in the magnitude of the RMS error. It is also possible to perform the calibration separately for different frequency bands. It should be noted, however, that this method of frequency-scale calibration uses all of the spectral data, not just peak positions, and therefore can only be employed with an etalon, where the spectral profile is well-defined, and is not applicable to measurements of absorption lines such as water vapour.

As seen in Fig. 5, the TDS frequency scale is correct within the measurement uncertainty. It should be noted, however, that in Fig. 5 the RMS error is calculated using the data in the range 0.2–2 THz, where the dynamic range of the system is above 100. The RMS error peak for both etalons is relatively shallow, so that the scale factor may be determined with an accuracy of $\sim$0.002. However, the dominant uncertainty is the etalon thickness.

5. Conclusion

We have demonstrated a simple and convenient method of frequency calibration for a TDS that provides a frequency check across the whole width of the measurement band. This has the advantage of revealing both systematic errors of the frequency scale, and errors arising from noise and frequency-dependent distortions. The method utilizes multiple reflection echoes, and for its implementation requires only an etalon with a well-defined and accurately known thickness. Unlike frequency standards using narrow-line absorption, such as gas absorption lines, this technique does not require high frequency resolution and/or low noise measurement.

Moreover, the RMS error calculation can also be used in reverse, in order to obtain the refractive index of thin samples or films.

Acknowledgment

The authors would like to thank the DIUS National Measurement System for financial support under its Physical Program.

References

[1] M.C. Beard, G.M. Turner, C.A. Schmuttenmaer, J. Phys. Chem. B 106 (2002) 7146.
[2] M. Hangyo, T. Nagashima, S. Nashima, Meas. Sci. Technol. 13 (2002) 1727.
[3] P.Y. Han, X.-C. Zhang, Meas. Sci. Technol. 12 (2001) 1747.
[4] H.J. Barker, G.C. Cho, H. Kurz, Q. Wu, X.-C. Zhang, J. Opt. Soc. Am. B 15 (1998) 1795.
[5] D.F. Williams et al., IEEE Trans. Microwave Theory and Tech. 54 (1) (2006) 481.
[6] A.J.A. Smith, A.G. Roddie, D. Henderson, Opt. Quant. Electron. 28 (1996) 933.
[7] R.J. Foltynowicz, R.E. Allman, Terahertz time-domain spectroscopy of atmospheric water vapor from 0.4 to 2.7 THz, Sandia Report, SND2005-5709, 2005.
[8] D.M. Mittleman, R.H. Jacobsen, R. Neelmani, R.G. Baraniuk, M.C. Nuss, Appl. Phys. B 67 (1998) 379.
[9] X. Xin, H. Altan, A. Saint, D. Matten, R.R. Alfano, J. Appl. Phys. 100 (2006) 094905.
[10] G. Zhao et al., Rev. Sci. Instrum. 73 (2002) 1715.
[11] M. Naftaly, R. Dudley, Opt. Lett. 34 (8) (2009) 1213.
[12] S. Mickan, J. Xu, J. Munch, X.-C. Zhang, D. Abbott, The limit of spectral resolution in THz time-domain spectroscopy, in: Proceedings of SPIE, vol. 5277 – 0277-786X/04/$15 – doi:10.1117/12.530386.
[13] T.D. Dorney, R.G. Baraniuk, D.M. Mittleman, J. Opt. Soc. Am. A 18 (7) (2001) 1562.
[14] W. Withayachumnankul, B. Ferguson, Fluctuation Noise Lett. 6 (2) (2006) L227.
[15] M. Naftaly, R.E. Miles, Opt. Commun. 280 (2007) 291.
[16] R. Guenther, Modern Optics, Wiley, 1990, ISBN 0-471-60538-7.
[17] J.R. Taylor, An Introduction to Error Analysis, Oxford University Press, 1982, ISBN 0-19-855707-8.
[18] D. Grischkowsy, S. Keiding, M. Van Exter, Ch. Fattinger, J. Opt. Soc. Am. B 7 (1990) 2006.
[19] J. Dai, J. Zhang, W. Zhang, D. Grischkowsky, J. Opt. Soc. Am. B 21 (2004) 1379.
[20] E.N. Grossman, D.G. McDonald, Opt. Eng. 34 (5) (1995) 1289.
[21] P. Kužel, M.A. Khazan, J. Kroupa, J. Opt. Soc. Am. B 16 (1999) 1795.
[22] L.S. Rothman et al., J. Quant. Spectrosc. Radiat. Transfer 110 (2009) 533.